Relative mass distributions of neutron-rich thermally fissile nuclei within a statistical model

Bharat Kumar,[1,2,*] M. T. Senthil Kannan,[3] M. Balasubramaniam,[3] B. K. Agrawal,[4,2] and S. K. Patra[1,2]
[1]*Institute of Physics, Sachivalaya Marg, Bhubaneswar 751005, India*
[2]*Homi Bhabha National Institute, Anushakti Nagar, Mumbai 400094, India*
[3]*Department of Physics, Bharathiar University, Coimbatore 641046, India*
[4]*Saha Institute of Nuclear Physics, 1/AF, Bidhannagar, Kolkata 700064, India*
(Received 12 June 2017; published 29 September 2017)

We study the binary mass distribution for the recently predicted thermally fissile neutron-rich uranium and thorium nuclei using a statistical model. The level density parameters needed for the study are evaluated from the excitation energies of the temperature-dependent relativistic mean field formalism. The excitation energy and the level density parameter for a given temperature are employed in the convolution integral method to obtain the probability of the particular fragmentation. As representative cases, we present the results for the binary yields of ^{250}U and ^{254}Th. The relative yields are presented for three different temperatures: $T = 1$, 2, and 3 MeV.

DOI: 10.1103/PhysRevC.96.034623

I. INTRODUCTION

The fission phenomenon is one of the most interesting subjects in the field of nuclear physics. To study fission properties, a large number of models have been proposed. The fissioning of a nucleus is successfully explained by the liquid drop model, and the semiempirical mass formula is the best and oldest simple tool to get a rough estimation of the energy released in a fission process. The pioneering work of Vautherin and Brink [1], who applied the Skyrme interaction in a self-consistent method for the calculation of ground state properties of finite nuclei, opened a new dimension in the quantitative estimation of nuclear properties. Subsequently, the Hartree-Fock and time-dependent Hartree-Fock formalisms [2] were also implemented to study the properties of fission. Most recently, the microscopic relativistic mean field approximation, which is another successful theory in nuclear physics, is also used for the study of nuclear fission [3].

In the last few decades, the availability of neutron-rich nuclei in various laboratories across the globe opened up new research in the field of nuclear physics, because of their exotic decay properties. The effort toward the synthesis of superheavy nuclei in laboratories such as Dubna (Russia), GSI (Germany), RIKEN (Japan) and BNL (USA) is also quite remarkable. Due to all these, the periodic table has been extended, to date, up to atomic number $Z = 118$ [4]. The decay modes of these superheavy nuclei are very different than the usual modes. Mostly, we understand that a neutron-rich nucleus has a larger number of neutron than nuclei in the light or medium mass region of the periodic table. The study of these neutron-rich superheavy nuclei is very interesting because of their ground state structures and various modes of decay, including multifragment fission (more than two fragments) [3]. Another interesting feature of some neutron-rich uranium and thorium nuclei is that, similar to ^{233}U, ^{235}U, and ^{239}Pu, the nuclei $^{246-264}$U and $^{244-262}$Th are also thermally fissile, which is extremely important for energy production in the fission process. If these neutron-rich uranium and thorium nuclei are viable sources, then these nuclei will be more effective for achieving the critical condition in a controlled fission reaction.

Now the question arises, how we can get a reasonable estimation of the mass yield in the spallation reaction of these neutron-rich thermally fissile nuclei? As mentioned earlier in this section, there are many formalisms available in the literature to study these cases. Here, we adopt the statistical model developed by Fong [5]. The calculation is further extended by Rajasekaran and Devanathan [6] to study the binary mass distributions using the single-particle energies of the Nilsson model. The obtained results are in good agreement with the experimental data. In the present study, we would like to replace the single-particle energies with the excitation energies of a successful microscopic approach: the relativistic mean field (RMF) formalism.

For the last few decades, the relativistic mean field (RMF) formalism [7–11] with various parameter sets has successfully reproduced the bulk properties, such as binding energies, root-mean-square radii, quadrupole deformation, etc., not only for nuclei near the β-stability line but also for nuclei away from it. Further, the RMF formalism has been successfully applied to the study of clusterization of known cluster emitting heavy nuclei [12–14] and the fission of hyper-hyper-deformed ^{56}Ni [15]. Rutz *et al.* [16] reproduced the double and triple humped fission barriers of ^{240}Pu and ^{232}Th and the asymmetric ground states of ^{226}Ra using the RMF formalism. Moreover, the symmetric and asymmetric fission modes are also successfully reproduced. Patra *et al.* [3] studied the neck configuration in the fission decay of neutron-rich U and Th isotopes. The main goal of this present paper is to understand the binary fragmentation yields of such neutron-rich thermally fissile superheavy nuclei. ^{250}U and ^{254}Th are taken for further calculations as the representative cases.

The paper is organized as follows: In Sec. II, the statistical model and relativistic mean field theory are presented briefly. In subsection II A, the level density parameter and it's relation with the relative mass yield are outlined. In subsection II B, the equation of motion of the nucleon and meson fields

*bharat@iopb.res.in

obtained from the relativistic mean field Lagrangian and the temperature dependence of the equations are adopted through the occupation numbers of protons and neutrons. The results are discussed in Sec. III and compared with the finite range droplet model (FRDM) predictions. The summary and concluding remarks are given in Sec. IV.

II. FORMALISM

The possible binary fragments of the considered nucleus are obtained by equating the charge-to-mass ratio of the parent nucleus to the fission fragments as [17]

$$\frac{Z_P}{A_P} \approx \frac{Z_i}{A_i}, \tag{1}$$

with A_P, Z_P and A_i, Z_i ($i = 1$ and 2) corresponding to mass and charge numbers of the parent nucleus and the fission fragments [6]. The constraints $A_1 + A_2 = A$, $Z_1 + Z_2 = Z$, and $A_1 \geqslant A_2$ are imposed to satisfy the conservation of charge and mass number in a nuclear fission process and to avoid the repetition of fission fragments. Another constraint, i.e., the binary charge numbers from $Z_2 \geqslant 26$ to $Z_1 \leqslant 66$, is also taken into consideration from the experimental yield [18] to generate the combinations, assuming that the fission fragments lie within these charge ranges.

A. Statistical theory

The statistical theory [5,19] assumes that the probability of the particular fragmentation is directly proportional to the folded level density ρ_{12} of the fragments with the total excitation energy E^*, i.e., $P(A_j,Z_j) \propto \rho_{12}(E^*)$. Here,

$$\rho_{12}(E^*) = \int_0^{E^*} \rho_1(E_1^*)\,\rho_2(E^* - E_1^*)\,dE_1^*, \tag{2}$$

and ρ_i is the level density of two fragments ($i = 1,2$). The nuclear level density [20,21] is expressed as a function of fragment excitation energy E_i^* and the single particle level density parameter a_i:

$$\rho_i(E_i^*) = \frac{1}{12}\left(\frac{\pi^2}{a_i}\right)^{1/4} E_i^{*(-5/4)} \exp(2\sqrt{a_i E_i^*}). \tag{3}$$

In Refs. [17,22], we calculate the excitation energies of the fragments using the ground state single-particle energies of finite range droplet model (FRDM) [23] at a given temperature T, keeping the total number of protons and neutrons fixed. In the present study, we apply the self consistent temperature dependent relativistic mean field theory to calculate the E^* of the fragments. The excitation energy is calculated as

$$E_i^*(T) = E_i(T) - E_i(T = 0). \tag{4}$$

The level density parameter a_i is given as

$$a_i = \frac{E_i^*}{T^2}. \tag{5}$$

The relative yield is calculated as the ratio of the probability of a given binary fragmentation to the sum of the probabilities of all the possible binary fragmentations:

$$Y(A_j,Z_j) = \frac{P(A_j,Z_j)}{\sum_j P(A_j,Z_j)}, \tag{6}$$

where A_j and Z_j refer to the binary fragmentations involving two fragments with mass and charge numbers A_1, A_2 and Z_1, Z_2 obtained from Eq. (1). The competing basic decay modes such as neutron/proton emission, α decay, and ternary fragmentation are not considered. In addition to these approximations, we have also not included the dynamics of the fission reaction, which are really important to get a quantitative comparison with the experimental measurements. The presented results are the prompt disintegration of a parent nucleus into two fragments (democratic breakup). The resulting excitation energy would be liberated as prompt particle emission or delayed emission, but such secondary emissions are also ignored.

B. RMF Formalism

The RMF theory assume that the nucleons interact with each other via meson fields. The nucleon-meson interaction is given by the Lagrangian density [7–9,11,24,25]

$$\begin{aligned}\mathcal{L} = {} & \overline{\psi_i}\{i\gamma^\mu\partial_\mu - M\}\psi_i + \frac{1}{2}\partial^\mu\sigma\partial_\mu\sigma - \frac{1}{2}m_\sigma^2\sigma^2 \\ & - \frac{1}{3}g_2\sigma^3 - \frac{1}{4}g_3\sigma^4 - g_\sigma\overline{\psi_i}\psi_i\sigma \\ & - \frac{1}{4}\Omega^{\mu\nu}\Omega_{\mu\nu} + \frac{1}{2}m_w^2V^\mu V_\mu - g_w\overline{\psi}_i\gamma^\mu\psi_i V_\mu \\ & - \frac{1}{4}\vec{B}^{\mu\nu}\cdot\vec{B}_{\mu\nu} + \frac{1}{2}m_\rho^2\vec{R}^\mu\cdot\vec{R}_\mu - g_\rho\overline{\psi}_i\gamma^\mu\vec{\tau}\psi_i\cdot\vec{R}^\mu \\ & - \frac{1}{4}F^{\mu\nu}F_{\mu\nu} - e\overline{\psi}_i\gamma^\mu\frac{(1-\tau_{3i})}{2}\psi_i A_\mu,\end{aligned} \tag{7}$$

where ψ_i is the single-particle Dirac spinor. The arrows over the letters in the above equation represent the isovector quantities. The nucleon and the σ, ω, and ρ meson masses are denoted by M, m_σ, m_ω, and m_ρ respectively. The meson and the photon fields are denoted as σ, V_μ, R^μ, and A_μ for σ, ω, ρ mesons and photon respectively. The g_σ, g_ω, g_ρ, and $\frac{e^2}{4\pi}$ are the coupling constants for the σ, ω, ρ mesons and photon fields with nucleons respectively. The strengths of the constants g_2 and g_3 are responsible for the nonlinear couplings of σ meson (σ^3 and σ^4). The field tensors of the isovector mesons and the photon are given by

$$\Omega^{\mu\nu} = \partial^\mu V^\nu - \partial^\nu V^\mu, \tag{8}$$

$$\vec{B}^{\mu\nu} = \partial^\mu\vec{R}^\nu - \partial^\nu\vec{R}^\mu - g_\rho(\vec{R}^\mu \times \vec{R}^\nu), \tag{9}$$

$$F^{\mu\nu} = \partial^\mu A^\nu - \partial^\nu A^\mu. \tag{10}$$

The classical variational principle gives the Euler-Lagrange equation and we get the Dirac equation with potential terms for the nucleons and Klein-Gordan equations with source terms for the mesons. We assume the no-sea approximation, so we neglect the antiparticle states. We are dealing with the static nucleus, so the time reversal symmetry and the conservation of parity simplifies the calculations. After simplifications, the

Dirac equation for the nucleon is given by

$$\{-i\alpha.\nabla + V(r) + \beta[M + S(r)]\}\,\psi_i = \epsilon_i\,\psi_i, \tag{11}$$

where $V(r)$ represents the vector potential and $S(r)$ is the scalar potential,

$$\begin{aligned} V(r) &= g_\omega\omega_0 + g_\rho\tau_3\rho_0(r) + e\frac{(1-\tau_3)}{2}A_0(r),\\ S(r) &= g_\sigma\sigma(r), \end{aligned} \tag{12}$$

which contributes to the effective mass,

$$M^*(r) = M + S(r). \tag{13}$$

The Klein-Gordon equations for the mesons and the electromagnetic fields with the nucleon densities as sources are

$$\{-\triangle + m_\sigma^2\}\sigma(r) = -g_\sigma\rho_s(r) - g_2\sigma^2(r) - g_3\sigma^3(r), \tag{14}$$

$$\{-\triangle + m_\omega^2\}\omega_0(r) = g_\omega\rho_v(r), \tag{15}$$

$$\{-\triangle + m_\rho^2\}\rho_0(r) = g_\rho\rho_3(r), \tag{16}$$

$$-\triangle A_0(r) = e\rho_c(r). \tag{17}$$

The corresponding densities such as scalar, baryon (vector), isovector, and proton (charge) are given as

$$\rho_s(r) = \sum_i n_i\,\psi_i^\dagger(r)\,\psi_i(r), \tag{18}$$

$$\rho_v(r) = \sum_i n_i\,\psi_i^\dagger(r)\,\gamma_0\,\psi_i(r), \tag{19}$$

$$\rho_3(r) = \sum_i n_i\,\psi_i^\dagger(r)\,\tau_3\,\psi_i(r), \tag{20}$$

$$\rho_c(r) = \sum_i n_i\,\psi_i^\dagger(r)\left(\frac{1-\tau_3}{2}\right)\psi_i(r). \tag{21}$$

To solve the Dirac and Klein-Gordan equations, we expand the Boson fields and the Dirac spinor in an axially deformed harmonic oscillator basis with β_0 as the initial deformation parameter. The nucleon equation along with different meson equations form a set of coupled equations, which can be solved by an iterative method. The center-of-mass correction is calculated with the nonrelativistic approximation. The quadrupole deformation parameter β_2 is calculated from the resulting quadrupole moments of the proton and neutron. The total energy is given by [10,26,27],

$$\begin{aligned} E(T) = \sum_i \epsilon_i n_i + E_\sigma + E_{\sigma NL} + E_\omega + E_\rho\\ + E_C + E_{\text{pair}} + E_{\text{c.m.}} - AM, \end{aligned} \tag{22}$$

with

$$E_\sigma = -\frac{1}{2}g_\sigma\int d^3r\,\rho_s(r)\sigma(r), \tag{23}$$

$$E_{\sigma NL} = -\frac{1}{2}\int d^3r\left\{\frac{2}{3}g_2\,\sigma^3(r) + \frac{1}{2}g_3\,\sigma^4(r)\right\}, \tag{24}$$

$$E_\omega = -\frac{1}{2}g_\omega\int d^3r\,\rho_v(r)\omega^0(r), \tag{25}$$

$$E_\rho = -\frac{1}{2}g_\rho\int d^3r\,\rho_3(r)\rho^0(r), \tag{26}$$

$$E_C = -\frac{e^2}{8\pi}\int d^3r\,\rho_c(r)A^0(r), \tag{27}$$

$$E_{\text{pair}} = -\triangle\sum_{i>0}u_i v_i = -\frac{\triangle^2}{G}, \tag{28}$$

$$E_{\text{c.m.}} = -\frac{3}{4}\times 41A^{-1/3}. \tag{29}$$

Here, ϵ_i is the single particle energy, n_i is the occupation probability, and E_{pair} is the pairing energy obtained from the simple BCS formalism.

C. Pairing and temperature-dependent RMF formalism

The pairing correlation plays a distinct role in open-shell nuclei. The effect of pairing correlation is markedly seen with increase in mass number A. Moreover, it helps in understanding the deformation of medium and heavy nuclei. It has a lean effect on both bulk and single-particles properties of lighter mass nuclei because of the availability of limited pairs near the Fermi surface. We take the case of the $T = 1$ channel of pairing correlation i.e,, pairing between proton-proton and neutron-neutron. In this case, a nucleon of quantum states $|jm_z\rangle$ pairs with another nucleons having the same I_z value with quantum states $|j - m_z\rangle$, since it is the time reversal partner of the other. In both nuclear and atomic domains the concept of BCS pairing is the same. The even-odd mass staggering of isotopes was the first evidence of its kind for the pairing energy. Considering the mean-field formalism, the violation of the particle number is seen only due to the pairing correlation. We find terms like $\psi^\dagger\psi$ (density) in the RMF Lagrangian density but we put an embargo on terms of the form $\psi^\dagger\psi^\dagger$ or $\psi\psi$ since they violate the particle number conservation. We apply externally the BCS constant pairing gap approximation for our calculation to take the pairing correlation into account. The pairing interaction energy in terms of occupation probabilities v_i^2 and $u_i^2 = 1 - v_i^2$ is written as [28,29]

$$E_{\text{pair}} = -G\left[\sum_{i>0}u_i v_i\right]^2, \tag{30}$$

with G being the pairing force constant. The variational approach with respect to the occupation number v_i^2 gives the BCS equation [29]

$$2\epsilon_i u_i v_i - \triangle\left(u_i^2 - v_i^2\right) = 0, \tag{31}$$

with the pairing gap $\triangle = G\sum_{i>0}u_i v_i$. The pairing gap ($\triangle$) of proton and neutron is taken from the empirical formula [10,30]:

$$\triangle = 12\times A^{-1/2}. \tag{32}$$

The temperature introduced in the partial occupancies in the BCS approximation is given by

$$n_i = v_i^2 = \frac{1}{2}\left[1 - \frac{\epsilon_i - \lambda}{\tilde{\epsilon_i}}[1 - 2f(\tilde{\epsilon_i},T)]\right], \tag{33}$$

with

$$f(\tilde{\epsilon}_i,T) = \frac{1}{(1+\exp[\tilde{\epsilon}_i/T])} \quad \text{and}$$
$$\tilde{\epsilon}_i = \sqrt{(\epsilon_i-\lambda)^2+\Delta^2}. \tag{34}$$

The function $f(\tilde{\epsilon}_i,T)$ represents the Fermi Dirac distribution for quasiparticle energy $\tilde{\epsilon}_i$. The chemical potential λ_p (λ_n) for protons (neutrons) is obtained from the constraints of particle number equations,

$$\sum_i n_i^Z = Z, \quad \sum_i n_i^N = N. \tag{35}$$

The sum is taken over all proton and neutron states. The entropy is obtained by

$$S = -\sum_i [n_i\, ln(n_i) + (1-n_i)\, ln(1-n_i)]. \tag{36}$$

The total energy and the gap parameter are obtained by minimizing the free energy,

$$F = E - TS. \tag{37}$$

In constant pairing gap calculations, for a particular value of pairing gap $\triangle$ and force constant G, the pairing energy E_{pair} diverges, if it is extended to an infinite configuration space. In fact, in all realistic calculations with finite range forces, $\triangle$ is not constant, but decreases with large angular momenta states above the Fermi surface. Therefore, a pairing window in all the equations is extended up to the level $|\epsilon_i - \lambda| \leqslant 2(41A^{-1/3})$ as a function of the single-particle energy. The factor 2 has been determined so as to reproduce the pairing correlation energy for neutrons in ^{118}Sn using the Gogny force [10,28,31].

III. RESULTS AND DISCUSSIONS

In our very recent work [32], we calculated the ternary mass distributions for ^{252}Cf, ^{242}Pu, and ^{236}U with the fixed third fragments A_3 = ^{48}Ca, ^{20}O, and ^{16}O respectively for the three different temperatures $T = 1$, 2, and 3 MeV within the TRMF formalism. The structure effects of binary fragments are also reported in Ref. [33]. In this article, we study the mass distribution of ^{250}U and ^{254}Th as representative cases from the range of neutron-rich thermally fissile nuclei $^{246-264}$U and $^{244-262}$Th. Because of the neutron-rich nature of these nuclei, a large number of neutrons are emitted during the fission process. These nucleons help to achieve the critical condition much sooner than in normal fissile nuclei.

To assure the predictability of the statistical model, we also study the binary fragmentation of naturally occurring ^{236}U and ^{232}Th nuclei. The possible binary fragments are obtained using the Eq. (1). To calculate the total binding energy at a given temperature, we use the axially symmetric harmonic oscillator basis expansions N_F and N_B for the Fermion and Boson wave functions to solve the Dirac equation (11) and the Klein-Gordon equations (14)–(17) iteratively. It is reported [34] that the effect of the basis space on the calculated binding energy, quadrupole deformation parameter (β_2), and the rms radii of the nucleus are almost equal for the basis set $N_F = N_B = 12$ to 20 in the mass region $A \sim 200$. Thus, we use the basis space $N_F = 12$ and $N_B = 20$ to study the binary fragments up to mass number $A \sim 182$. The binding energy is obtained by minimizing the free energy, which gives the most probable quadrupole deformation parameter β_2 and the proton (neutron) pairing gaps $\triangle_p$ ($\triangle_n$) for the given temperature. At finite temperature, the continuum corrections due to the excitation of nucleons need to be considered. The level density in the continuum depends on the basis space N_F and N_B [35]. It is shown that the continuum corrections need not be included in the calculations of level densities up to the temperature $T \sim 3$ MeV [36,37].

A. Level density parameter and level density within TRMF and FRDM formalisms

In TRMF, the excitation energies E^* and the level density parameters a_i of the fragments are obtained self-consistently from Eqs. (4) and (5). The FRDM calculations are also done for comparison. In this case, level densities of the fragments are evaluated from the ground state single-particle energies of the finite range droplet model (FRDM) of Möller *et al.* [38] which are retrieved from the Reference Input Parameter Library (RIPL-3) [39]. The total energy at a given temperature is calculated as $E(T) = \sum n_i\epsilon_i$; ϵ_i are the ground state single-particle energies and n_i are the Fermi-Dirac distribution functions. The T-dependent energies are obtained by varying the occupation numbers at a fixed particle number for a given temperature and given fragment. The level density parameter a is a crucial quantity in the statistical theory for the estimation of yields. These values of a for the binary fragments of ^{236}U, ^{250}U, ^{232}Th, and ^{254}Th obtained from TRMF and FRDM are depicted in Fig. 1. The empirical estimations $a = A/K$ are also given for comparison, with K being the inverse level density parameter. In general, the K value varies from 8 to 13 with the increasing temperature. However, the level density parameter is considered to be constant up to $T \approx 4$ MeV. Hence, we take the practical value of $K = 10$ as mentioned in Ref. [40]. The a values of TRMF are close to the empirical level density parameter. The FRDM level density parameters are appreciably lower than the referenced a. Further, in both models at $T = 1$ MeV, there are more fluctuations in the level density parameter due to the shell effects of the fragments. At $T = 2$ and 3 MeV, the variations are small. This may be due to the fact that the shell becomes degenerate at the higher temperatures. All fragments becomes spherical at temperature $T \approx 3$ MeV as shown in Ref. [33].

The level density parameter a is evaluated in two different ways using excitation energy and the entropy of the system as

$$a_E = \frac{E^*}{T^2}, \quad a_S = \frac{S}{2T}. \tag{38}$$

For instance, the inverse level density parameters K_E and K_S of ^{236}U, ^{250}U, ^{232}Th, and ^{254}Th within the TRMF formalism are depicted in Fig. 2. Both K_S and K_E have maximum fluctuation up to 30 MeV at $T = 1$ MeV. These values reduce to 10–13 MeV at temperature $T = 2$ MeV or above. It is

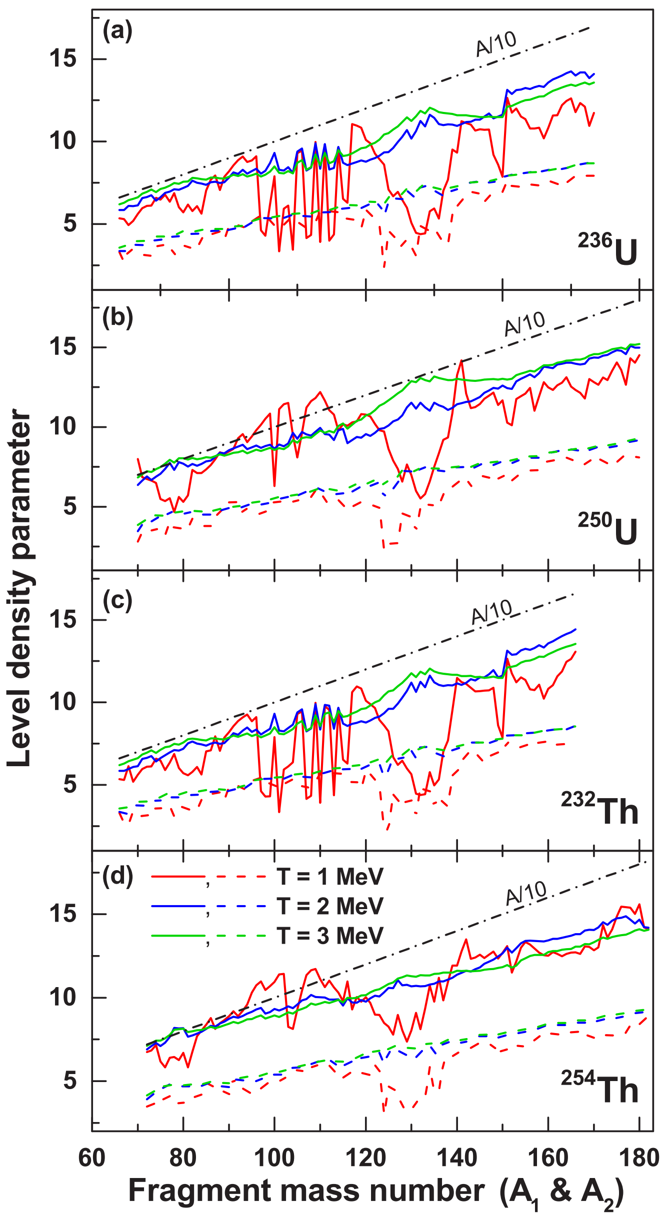

FIG. 1. The level density parameter a for the binary fragmentation of ^{236}U, ^{250}U, ^{232}Th, and ^{254}Th at temperatures $T = 1$, 2, and 3 MeV within the TRMF (solid lines) and FRDM (dashed lines) formalisms.

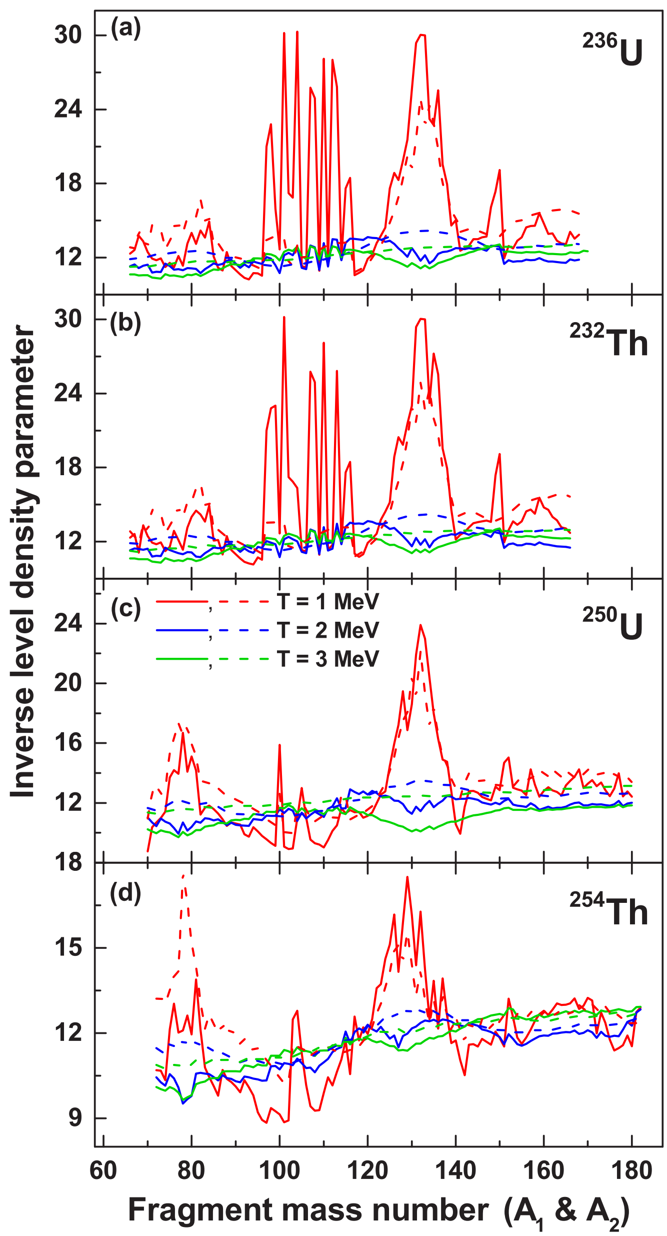

FIG. 2. The inverse level density parameters K_E (solid lines) and K_S (dashed lines) are obtained for ^{236}U, ^{250}U, ^{232}Th, and ^{254}Th at temperatures $T = 1$, 2, and 3 MeV.

to be noted that, at $T = 3$ MeV, the inverse level density parameter is substantially lower around the mass number $A \sim 130$ in all cases. This may be due to the neutron closed shell ($N = 82$) in the fission fragments of ^{236}U and ^{232}Th and the neutron-rich nuclei ^{250}U and ^{254}Th. The level densities for the fission fragments of ^{236}U, ^{250}U, ^{232}Th, and ^{254}Th are plotted as a function of mass number in Fig. 3 within the TRMF and FRDM formalisms at three different temperatures, $T = 1$, 2, and 3 MeV.

The level density ρ has maximum fluctuations at $T = 1$ MeV for all considered nuclei in the TRMF model, similar to the level density parameter a. The ρ values are substantially lower at mass number $A \sim 130$ for all nuclei. In Fig. 3, one can notice that the level density has small kinks in the mass regions $A \sim 71$–81 of ^{236}U and $A \sim 77$–91 of ^{250}U, compared with the neighboring nuclei at temperature $T = 2$ MeV. Consequently, the corresponding partner fragments have also higher ρ values. A further inspection reveals that the level density of the closed shell nucleus around $A \sim 130$ has higher value than the neighboring nuclei for both ^{236,250}U, but it has lower yield due to the smaller level density of the corresponding partners. At $T = 3$ MeV, the level density of the fragments around mass numbers $A \sim 72$ and 130 have larger values compared to other fragments of ^{236}U. On the other hand, the level density in the vicinity of neutron number $N = 82$ and proton number $Z = 50$ for the fragments of the neutron-rich ^{250}U nucleus is quite high,

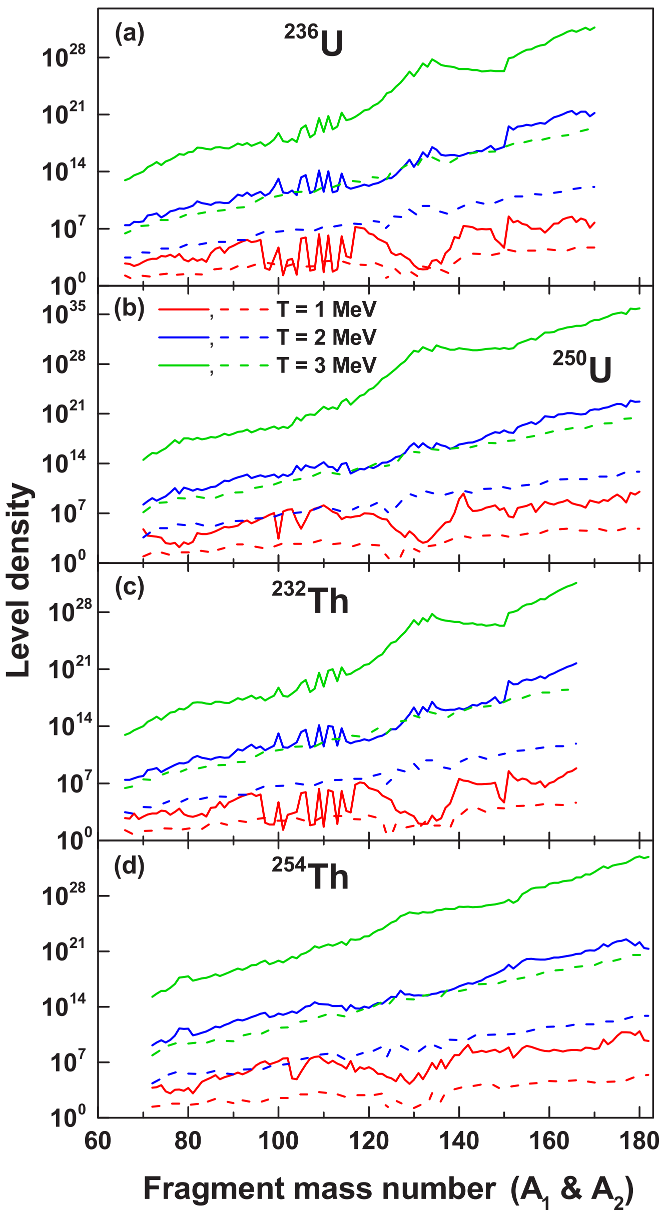

FIG. 3. The level densities of the binary fragmentations of ^{236}U, ^{250}U, ^{232}Th, and ^{254}Th at temperatures $T = 1$, 2, and 3 MeV within the TRMF (solid lines) and FRDM (dashed lines) formalisms.

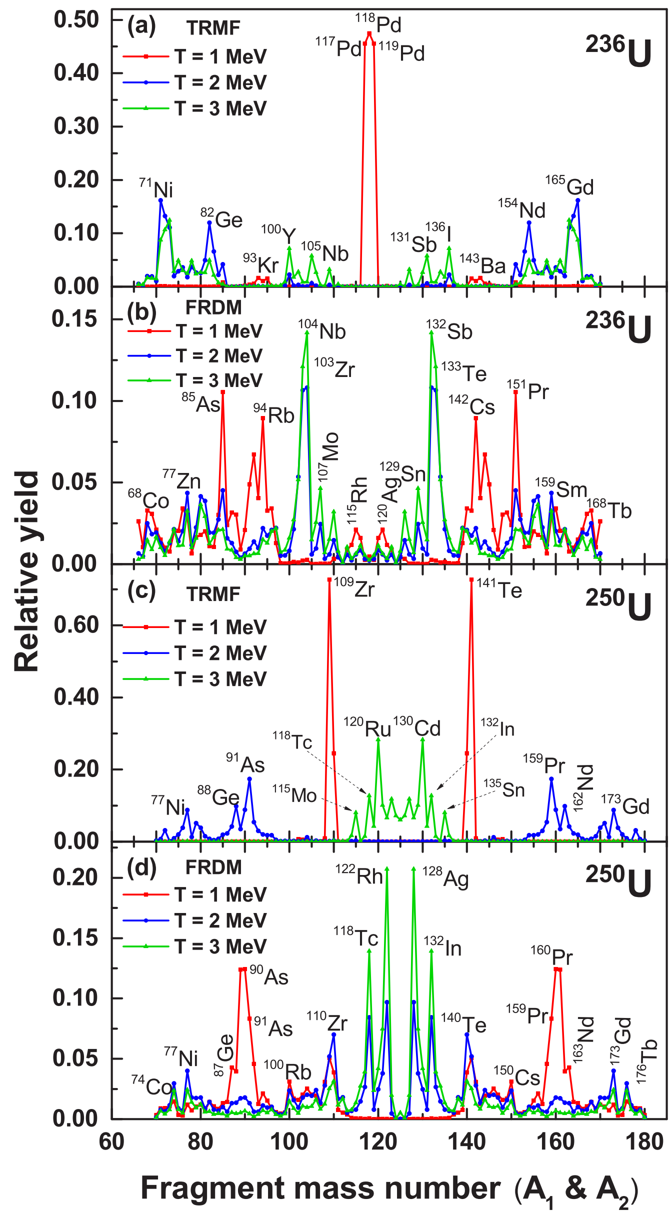

FIG. 4. Mass distributions of ^{236}U and ^{250}U at temperatures $T = 1$, 2, and 3 MeV. The total yield values are normalized to the scale 2.

because of the closed shell of the fragments. This is evident from the small kink in the level density of ^{130}Cd ($N = 82$), ^{132}In($N \sim 82$), and ^{135}Sn ($Z = 50$). Again, for ^{232}Th, the level densities are found to be maximum at around mass number $A \sim 81$ and 100 for $T = 2$ MeV. In case of ^{254}Th, the ρ values are found to be large for the fragments around $A \sim 78$ and 97 at $T = 2$ MeV. Their corresponding partners have also similar behavior. For higher temperature $T = 3$ MeV, the higher ρ values of ^{232}Th fragments are notable around mass number $A \sim 130$. Similarly, for ^{254}Th, the fission fragments around $A \sim 78$ have higher level density at $T = 3$ MeV. In general, the level density increases towards the neutron closed shell ($N = 82$) nucleus.

B. Relative fragmentation distribution in binary systems

In this section, the mass distributions of ^{236}U, ^{232}Th, and the neutron-rich nuclei ^{250}U and ^{254}Th are calculated at temperatures $T = 1$, 2, and 3 MeV using TRMF and FRDM excitation energies and the level density parameters a as explained in Sec. II. The binary mass distributions of ^{236,250}U and ^{232,254}Th are plotted in Figs. 4 and 5. The total energy at finite temperature and ground state energy are calculated using the TRMF formalism as discussed in Sec. III A. From the excitation energy E^* and the temperature T, the level density parameter a and the level density ρ of the fragments are calculated using Eq. (3). From the fragment level densities ρ_i, the folding density ρ_{12} is calculated using the convolution integral

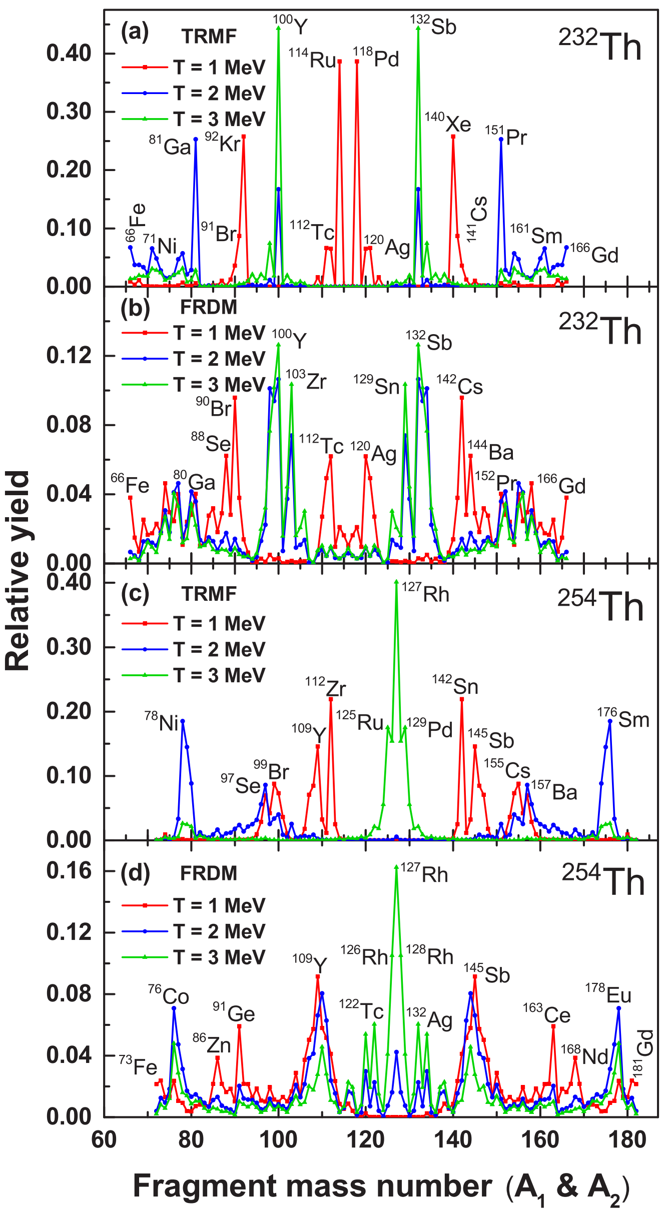

FIG. 5. Mass distributions of ^{232}Th and ^{254}Th at temperatures $T = 1$, 2, and 3 MeV. The total yield values are normalized to the scale 2.

as in Eq. (2) and the relative yields are calculated using Eq. (6). The total yields are normalized to the scale 2.

The mass yields of normal nuclei ^{236}U and ^{232}Th are briefly explained first, followed by a detailed description of the neutron-rich nuclei. The results of the most favorable fragment yields of ^{236,250}U and ^{232,254}Th are listed in Table I at three different temperatures, $T = 1$, 2, and 3 MeV, for both TRMF and FRDM formalisms. From Figs. 4 and 5, it is shown that the mass distributions for ^{236}U and ^{232}Th are quite different from those of the neutron-rich ^{250}U and ^{254}Th isotopes.

The symmetric binary fragmentation ^{118}Pd + ^{118}Pd for ^{236}U is the most favorable combination. In TRMF, the fragments with closed shell ($N = 100$ and $Z = 28$) combinations are more probable at the temperature $T = 2$ MeV. The blend region of neutron and proton closed shells ($N \approx 82$ and $Z \approx 50$) has considerable yield values at $T = 3$ MeV. The fragmentations ^{151}Pr + ^{85}As, ^{142}Cs + ^{94}Rb, and ^{144}Ba + ^{92}Kr are the favorable combinations at temperature $T = 1$ MeV in the FRDM formalism. For higher temperatures $T = 2$ and 3 MeV, the closed shell or nearly closed shell fragments ($N = 82,50$ and $Z = 28$) have larger yields. From Fig. 5, the in TRMF formalism, the combinations ^{118}Pd + ^{114}Ru and ^{140}Xe + ^{92}Kr are the possible fragments at $T = 1$ MeV for the nucleus ^{232}Th. At $T = 2$ MeV, we find maximum yields for the fragments with the closed shell or nearly closed shell combinations ($N = 82,50$). For higher temperature $T = 3$ MeV, near the neutron closed shell ($N \sim 82$), ^{132}Sb + ^{100}Y is the most favorable fragmentation pair compared with all other yields. Similar fragmentations are found in the FRDM formalism at $T = 2$ and 3 MeV. In addition, the probability of the evaluation of ^{129}Sn + ^{103}Zr is also quite substantial in the fission process. For $T = 1$ MeV, the yield is more or less similar to the TRMF model.

From Fig. 4, for ^{250}U the fragment combinations ^{140,141}Te + ^{110,109}Zr have the maximum yields at $T = 1$ MeV in TRMF. This is also consistent with the evolution of the subclosed proton shell $Z = 40$ in Zr isotopes [41]. Contrary to this almost symmetric binary yield, the mass distribution of this nucleus in the FRDM formalism has an asymmetric evolution of fragment combinations such as ^{160,159}Pr + ^{90,91}As, ^{163,162}Nd + ^{87,88}Ge, and ^{150}Cs + ^{100}Rb. Interestingly, at $T = 2$ and 3 MeV, the more favorable fragment combinations have one of the closed shell nuclei. At $T = 2$ MeV, ^{159}Pr + ^{91}As, ^{162}Nd + ^{88}Ge, and ^{173}Gd + ^{77}Ni are the more probable fragmentations [see Fig. 4(c)]. It is reported by Satpathy *et al.* [42] and experimentally verified by Patel *et al.* [43] that $N = 100$ is a neutron close shell for the deformed region, where $Z = 62$ acts like a magic number. In FRDM, ^{128}Ag + ^{122}Rh, ^{132}In + ^{118}Tc, ^{140}Te + ^{110}Zr, and ^{173}Gd + ^{77}Ni have larger yields at temperature $T = 2$ MeV. With the TRMF method, the most favorable fragments are confined in the single region ($A \approx 114$–136) which is a blend of vicinities of neutron ($N = 82$) and proton ($Z = 50$) closed shell nuclei at $T = 3$ MeV. The fragment combinations ^{130}Cd + ^{120}Ru, ^{132}In + ^{118}Tc, and ^{135}Sn + ^{115}Mo are the major yields for ^{250}U at $T = 3$ MeV in TRMF calculations. With the FRDM method, at $T = 3$ MeV, more probable fragments are similar to those at $T = 2$ MeV. A comparison between Figs. 4(c) and 4(d) clarifies that, although the predictions of FRDM and TRMF at $T = 3$ MeV are qualitatively similar, they are quantitatively very different at $T = 2$ MeV in both the predictions. Also, from Fig. 4, it is inferred that the yields of the fragment combinations in the blend region increase and in other region decrease at $T = 2$ MeV.

In the present study, the total energy of the parent nucleus A is more than the sum of the energies of the daughters A_1 and A_2. Here, the dynamics of the entire process starting from the initial stage up to the scission are ignored. As a result, the energy conservation in the spallation reaction is not taken into account. The fragment yield can be regarded as the relative fragmentation probability, which is obtained from Eq. (6). Now we analyze the fragmentation yields for Th isotopes, and the results are depicted in Fig. 5 and Table I. In this case, one

TABLE I. The relative fragmentation yield (R.Y.) = $Y(A_j,Z_j) = \frac{P(A_j,Z_j)}{\sum P(A_j,Z_j)}$ for ^{236}U, ^{250}U, ^{232}Th, and ^{254}Th, obtained with TRMF at temperatures $T = 1$, 2, and 3 MeV are compared with the FRDM prediction (the yield values are normalized to 2).

Parent	T (MeV)	TRMF		FRDM		Parent	T (MeV)	TRMF		FRDM	
		Fragment	R.Y.	Fragment	R.Y.			Fragment	R.Y.	Fragment	R.Y.
^{236}U	1	^{118}Pd + ^{118}Pd	0.949	^{151}Pr + ^{85}As	0.210	^{250}U	1	^{141}Te + ^{109}Zr	1.454	^{160}Pr + ^{90}As	0.248
		^{119}Pd + ^{117}Pd	0.910	^{142}Cs + ^{94}Rb	0.178			^{140}Te + ^{110}Zr	0.491	^{161}Pr + ^{89}As	0.247
		^{143}Ba + ^{93}Kr	0.032	^{144}Ba + ^{92}Kr	0.134			^{148}Xe + ^{102}Sr	0.014	^{159}Pr + ^{91}As	0.166
	2	^{165}Gd + ^{71}Ni	0.323	^{132}Sb + ^{104}Nb	0.216		2	^{159}Pr + ^{91}As	0.348	^{128}Ag + ^{122}Rh	0.193
		^{164}Gd + ^{72}Ni	0.264	^{133}Te + ^{103}Zr	0.213			^{162}Nd + ^{88}Ge	0.197	^{132}In + ^{118}Tc	0.168
		^{163}Gd + ^{73}Ni	0.221	^{151}Pr + ^{85}As	0.210			^{160}Pr + ^{90}As	0.176	^{140}Te + ^{110}Zn	0.140
		^{154}Nd + ^{82}Ge	0.240	^{159}Sb + ^{77}Zn	0.087			^{173}Gd + ^{77}Ni	0.175	^{141}Te + ^{109}Zn	0.100
	3	^{163}Gd + ^{73}Ni	0.249	^{132}Sb + ^{104}Nb	0.283		3	^{130}Cd + ^{120}Ru	0.565	^{128}Ag + ^{122}Rh	0.414
		^{164}Gd + ^{72}Ni	0.214	^{133}Te + ^{103}Zr	0.242			^{132}In + ^{118}Tc	0.255	^{132}In + ^{118}Tc	0.278
		^{136}I + ^{100}Y	0.143	^{134}Te + ^{102}Zr	0.102			^{127}Ag + ^{123}Rh	0.236	^{129}Ag + ^{121}Rh	0.149
		^{131}Sb + ^{105}Nb	0.114	^{129}Sn + ^{107}Mo	0.092			^{135}Sn + ^{115}Mo	0.161	^{130}Cd + ^{120}Ru	0.083
^{232}Th	1	^{118}Pd + ^{114}Ru	0.773	^{142}Cs + ^{90}Br	0.190	^{254}Th	1	^{142}Sn + ^{112}Zr	0.439	^{145}Sb + ^{109}Y	0.183
		^{140}Xe + ^{92}Kr	0.515	^{144}Ba + ^{88}Se	0.124			^{145}Sb + ^{109}Y	0.291	^{163}Ce + ^{91}Ge	0.118
		^{141}Cs + ^{91}Br	0.174	^{120}Ag + ^{112}Tc	0.123			^{155}Cs + ^{99}Br	0.176	^{144}Sb + ^{110}Y	0.115
		^{120}Ag + ^{112}Tc	0.129	^{158}Pm + ^{74}Cu	0.092			^{157}Ba + ^{97}Se	0.139	^{168}Nd + ^{86}Zn	0.077
	2	^{151}Pr + ^{81}Ga	0.505	^{132}Sb + ^{100}Y	0.213		2	^{176}Sm + ^{78}Ni	0.370	^{144}Sb + ^{110}Y	0.161
		^{132}Sb + ^{100}Y	0.334	^{134}Te + ^{98}Sr	0.202			^{175}Sm + ^{79}Ni	0.290	^{178}Eu + ^{76}Co	0.141
		^{166}Gd + ^{66}Fe	0.134	^{129}Sn + ^{103}Zr	0.146			^{157}Ba + ^{97}Se	0.172	^{144}Sb + ^{110}Y	0.132
	3	^{132}Sb + ^{100}Y	0.886	^{132}Sb + ^{100}Y	0.252		3	^{127}Rh + ^{127}Rh	0.803	^{127}Rh + ^{127}Rh	0.325
		^{134}Te + ^{98}Sr	0.148	^{129}Sn + ^{103}Zr	0.207			^{129}Pd + ^{125}Ru	0.350	^{127}Rh + ^{127}Rh	0.210
		^{155}Nd + ^{77}Zn	0.063	^{134}Te + ^{98}Sr	0.153			^{128}Rh + ^{126}Rh	0.307	^{132}Ag + ^{122}Tc	0.120

can see that the mass distribution broadly spreads throughout the region $A_i = 66$–166. Again, the most concentrated yields can be divided into two regions, I ($A_1 = 141$–148 and $A_2 = 106$–113) and II ($A_1 = 152$–158 and $A_2 = 102$–96), for ^{254}Th in the TRMF formalism at the temperature $T = 1$ MeV. The most favorable fragmentation ^{142}Sn + ^{112}Zr is obtained from region I. The other combinations in that region have also considerable yields. In region II, the isotopes of Ba and Cs appear, curiously, along with their corresponding partners. Categorically, in FRDM predictions, region I has larger yields at $T = 1$ MeV. The other possible fragmentations are ^{163}Ce + ^{91}Ge, ^{168}Nd + ^{86}Zn, and ^{181}Gd + ^{73}Fe [see Figs. 5(b) and 5(d)]. The mass distribution is different with different temperature, and the maximum yields at $T = 2$ MeV in the TRMF formalism are ^{174,175,176}Sm + ^{80,79,78}Ni. Apart from these combinations, there are other considerable yields as can be seen in Fig. 5 for region II. The prediction of maximum probability of the fragment productions with the FRDM method are ^{144}Sb + ^{110}Y, ^{178}Eu + ^{76}Co, and ^{127}Rh + ^{127}Rh at $T = 2$ MeV. Besides these yields, one can find other notable evolutions of masses in region I due to the vicinity of the proton closed shell. Interestingly, at $T = 3$ MeV, the symmetric binary combination ^{127}Rh + ^{127}Rh has the largest yield due to the neutron closed shell ($N = 82$) of the fragment ^{127}Rh. The other yield fragments have an exactly or nearly a magic nucleon combination, mostly neutron ($N = 82$), as one of the fragments. A considerable yield is also seen for the proton close shell ($Z = 28$) Ni and/or ($Z = 62$) Sm isotopes, supporting our earlier prediction [33]. This confirms the prediction of Sm as a deformed magic nucleus [42,43]. Another observation of the present calculations show that the yields of the neutron-rich nuclei agree with the symmetric mass distribution of Chaudhuri *et al.* [44] at large excitation energy, which contradicts the recent prediction of a large asymmetric mass distribution of neutron-deficient Th isotopes [45]. These two results [44,45] along with our present calculations confirm that the symmetric or asymmetric mass distribution at different temperature depends on the proton and neutron combination of the parent nucleus. In general, both TRMF and FRDM predict maximum yields for both symmetric and asymmetric binary fragmentations followed by other secondary fragmentation emissions, depending on the temperature as well as the mass number of the parent nucleus. Thus, the binary fragments have larger level density ρ comparing with other nuclei because of neutron/proton close shell fragment combinations at $T = 2$ and 3 MeV. This result is consistent with the fact that most favorable fragments have larger phase space than the neighboring nuclei, as reported earlier [32,33].

To this end, it may be mentioned that the differences in the mass distributions or the relative yields calculated using TRMF and FRDM approaches mainly arise due to the differences in the level densities associated with these approaches. The mean values and the fluctuations in the level density parameter and the corresponding level density are even qualitatively different in the two approaches considered. This possibly stems from the fact that the single-particle energies in the FRDM are temperature independent. The temperature dependence of the excitation energy, required to calculate the level density parameter, comes only from the modification of the single-particle occupancy due to the Fermi distribution. In the TRMF approach, the excitation energy for each fragment at a given temperature is calculated self-consistently. Therefore, the deformation and the single-particle energies changes with temperature.

For the neutron-rich nuclei, the fragments having neutron/proton close shells $N = 50$, 82, and 100 have maximum possibility of emission at $T = 2$ and 3 MeV (for both nuclei ^{250}U and ^{254}Th). This is a general trend we could expect for all neutron-rich nuclei. It is worthwhile to mention some of the recent reports and predictions of multifragment fission for neutron-rich uranium and thorium nuclei. When such a neutron-rich nucleus breaks into two fragments, the products exceed the drip-line, leaving few nucleons (or light nuclei) free. As a result, these free particles along with the scission neutrons enhance the chain reaction in a thermonuclear device. These additional particles (nucleons or light nuclei) are responsible for reaching the critical condition much faster than in the usual fission for a normal thermally fissile nucleus. Thus, neutron-rich thermally fissile nuclei, such as $^{246–264}$U and $^{244–262}$Th, will be very useful for energy production.

IV. SUMMARY AND CONCLUSIONS

The fission mass distributions of β-stable nuclei ^{236}U and ^{232}Th and the neutron-rich thermally fissile nuclei ^{250}U and ^{254}Th are studied within a statistical model. The possible combinations are obtained by equating the charge-to-mass ratio of the parents to that of the fragments. The excitation energies of fragments are evaluated from the temperature-dependent self-consistent binding energies at the given T and the ground state binding energies which are calculated from the relativistic mean field model. The level densities and the yield combinations are manipulated using the convolution integral approach. The fission mass distributions of the aforementioned nuclei are also evaluated using the FRDM formalism for comparison. The level density parameter a and inverse level density parameter K are also studied to see the difference between results with these two methods. Besides fission fragments, the level densities are also discussed in the present paper. For ^{236}U and ^{232}Th, the symmetric and nearly symmetric fragmentations are more favorable at temperature $T = 1$ MeV. Interestingly, in most of the cases we find that one of the favorable fragments has a closed shell or nearly closed shell configuration ($N = 82$, 50 and $Z = 28$) at temperatures $T = 2$ and 3 MeV. This result agrees with our earlier predictions. Further, Zr isotopes have larger yield values for ^{250}U and ^{254}Th with their accompanying possible fragments at $T = 1$ MeV. The Ba and Cs isotopes with their partners are also more possible for ^{254}Th. This could be due to the deformed close shell in the region $Z = 52$–66 of the periodic table [46]. The Ni isotopes and the neutron closed shell ($N \sim 100$) nuclei are some of the prominent yields for both ^{250}U and ^{254}Th at temperature $T = 2$ MeV. At $T = 3$ MeV, the neutron closed shell ($N = 82$) is one of the largest yield fragments. The symmetric fragmentation ^{127}Rh + ^{127}Rh is possible for ^{254}Th due to the $N = 82$ closed shell occurring in binary fragmentation. For ^{250}U, the larger yield values are confined to the junction of neutron and proton closed shell nuclei.

ACKNOWLEDGMENTS

M.T.S. acknowledges financial support from UGC research grant, letter no. F.25-1/2014-15(BSR)7-307/2010/(BSR) dated 05.11.2015, and Institute Of Physics, Bhubaneswar for warm hospitality and for providing the necessary computer facilities.

[1] D. Vautherin and D. M. Brink, Phys. Lett. B **32**, 149 (1970); Phys. Rev. C **5**, 626 (1972).
[2] M. K. Pal and A. P. Stamp, Nucl. Phys. A **99**, 228 (1967).
[3] S. K. Patra, R. K. Choudhury, and L. Satpathy, J. Phys. G. **37**, 085103 (2010).
[4] M. Wang, G. Audi, A. H. Wapstra, F. G. Kondev, M. MacCromick, X. Xu, and B. Pfeiffer, Chin. Phys. C **36**, 1603 (2012).
[5] P. Fong, Phys. Rev. **102**, 434 (1956).
[6] M. Rajasekaran and V. Devanathan, Phys. Rev. C **24**, 2606 (1981).
[7] J. D. Walecka, Ann. Phys. (NY) **83**, 491 (1974).
[8] C. J. Horowitz and B. D. Serot, Nucl. Phys. A **368**, 503 (1981).
[9] B. D. Serot and J. D. Walecka, in *Advances in Nuclear Physics 16*, edited by J. W. Negele and E. Vogt (Plenum Press, New York, 1986), p. 1.
[10] Y. K. Gambhir, P. Ring, and A. Thimet, Ann. Phys. (NY) **198**, 132 (1990).
[11] S. K. Patra and C. R. Praharaj, Phys. Rev. C **44**, 2552 (1991).
[12] P. Arumugam, B. K. Sharma, S. K. Patra, and R. K. Gupta, Phys. Rev. C **71**, 064308 (2005).
[13] B. K. Sharma, P. Arumugam, S. K. Patra, P. D. Stevenson, R. K. Gupta, and W. Greiner, J. Phys. G. **32**, L1 (2006).
[14] S. K. Patra, Raj. K. Gupta, B. K. Sharma, P. D. Stevenson, and W. Greiner, J. Phys. G. **34**, 2073 (2007).
[15] R. K. Gupta, S. K. Patra, P. D. Stevenson, C. Beck, and W. Greiner, J. Phys. G. **35**, 075106 (2008).
[16] K. Rutz, J. A. Maruhn, P.-G. Reinhard, and W. Greiner, Nucl. Phys. A **590**, 680 (1995).
[17] M. Balasubramaniam, C. Karthikraj, S. Selvaraj, and N. Arunachalam, Phys. Rev. C **90**, 054611 (2014).
[18] D. W. Bergen and R. R. Fullwood, Nucl. Phys. A **163**, 577 (1971).
[19] A. J. Cole, in *Fundamental and Applied Nuclear Physics Series - Statistical Models for Nuclear Decay From Evaporation to Vaporization*, edited by R. R. Betts and W. Greiner (Institute of Physics, Bristol, 2000).
[20] J. R. Huizenga and L. G. Moretto, Annu. Rev. Nucl. Sci. **22**, 427 (1972).
[21] H. Bethe, Rev. Mod. Phys. **9**, 69 (1937).
[22] M. T. Senthil Kannan and M. Balasubramaniam, Eur. Phys. J. A **53**, 164 (2017).
[23] P. Möller, J. R. Nix, W. D. Myers, and W. J. Swiatecki, At. Data Nucl. Data Tables **66**, 131 (1997).
[24] J. Boguta and A. R. Bodmer, Nucl. Phys. A **292**, 413 (1977).

[25] C. E. Price and G. E. Walker, Phys. Rev. C **36**, 354 (1987).
[26] P. G. Blunden and M. J. Iqbal, Phys. Lett. B **196**, 295 (1987).
[27] P. G. Reinhard, Rep. Prog. Phys. **52**, 439 (1989).
[28] S. K. Patra, Phys. Rev. C **48**, 1449 (1993).
[29] M. A. Preston and R. K. Bhaduri, *Structure of the Nucleus* (Addison-Wesley, Reading, MA, 1982), Chap. 8, p. 309.
[30] D. Vautherin, Phys. Rev. C **7**, 296 (1973).
[31] J. Dechargé and D. Gogny, Phys. Rev. C **21**, 1568 (1980).
[32] M. T. Senthil Kannan, B. Kumar, M. Balasubramaniam, B. K. Agrawal, and S. K. Patra, Phys. Rev. C **95**, 064613 (2017).
[33] B. Kumar, M. T. Senthil Kannan, M. Balasubramaniam, B. K. Agrawal, and S. K. Patra, arXiv:1701.00731.
[34] B. Kumar, S. K. Biswal, S. K. Singh, and S. K. Patra, Phys. Rev. C **92**, 054314 (2015).
[35] Y.-F. Niu, H.-Z. Linag, and J. Meng, Chin. Phys. Lett. **26**, 032103 (2009).
[36] B. K. Agrawal, T. Sil, J. N. De, and S. K. Samaddar, Phys. Rev. C **62**, 044307 (2000); **63**, 024002 (2001).
[37] B. K. Agrawal, S. K. Samaddar, J. N. De, and S. Shlomo, Phys. Rev. C **58**, 3004 (1998).
[38] P. Möller, J. R. Nix, and K. L. Kratz, At. Data Nucl. Data Tables **59**, 185 (1995).
[39] https://www-nds.iaea.org/RIPL-3/.
[40] B. Nerlo-Pomorska, K. Pomorski, J. Bartel, and K. Dietrich, Phys. Rev. C **66**, 051302(R) (2002).
[41] J. M. Blatt and V. F. Weisskopf, *Theoretical Nuclear Physics* (Dover, Mineola, NY, 1991).
[42] L. Satpathy and S. K. Patra, J. Phys. G **30**, 771 (2004).
[43] Z. Patel *et al.*, Phys. Rev. Lett. **113**, 262502 (2014).
[44] A. Chaudhuri, T. K. Ghosh, K. Banerjee, S. Bhattacharya, J. Sadhukhan, C. Bhattacharya, S. Kundu, J. K. Meena, G. Mukherjee, R. Pandey, T. K. Rana, P. Roy, T. Roy, V. Srivastava, and P. Bhattacharya, Phys. Rev. C **91**, 044620 (2015).
[45] H. Paşca, A. V. Andreev, G. G. Adamian, and N. V. Antonenko, Phys. Rev. C **94**, 064614 (2016).
[46] E. F. Jones *et al.*, J. Phys. G **30**, L43 (2004).